Journal of Catalysis **193,** 123–131 (2000)
doi:10.1006/jcat.2000.2873, available online at http://www.idealibrary.com on IDEAL®

Selective Hydrodesulfurization of FCC Naphtha with Supported MoS_2 Catalysts: The Role of Cobalt

J. T. Miller,*,[1] W. J. Reagan,* J. A. Kaduk,* C. L. Marshall,† and A. J. Kropf†

*BP Amoco Research Center, E-1F, 150 West Warrenville Road, Naperville, Illinois 60563; and †Argonne National Laboratory, Chemical Technology Division, 9700 Cass Avenue, Argonne, Illinois 60439-4837

Received December 21, 1999; accepted March 15, 2000

The catalytic activity and selectivity for hydrodesulfurization (HDS) and olefin hydrogenation of FCC naphtha have been determined for MoS_2 (no Co) catalysts on different supports and for a commercial CoMo/alumina HDS catalyst both with and without the addition of alkali. For MoS_2 catalysts, the specific HDS activity is higher on silica than alumina, while addition of Cs resulted in no change in the activity. The differences in activity, however, are relatively small, a factor of less than two. EXAFS and XRD structural analysis indicate that small MoS_2 particles are present on all catalysts. The differences in rate are not due to differences in particle size, dispersion, or support physical properties, but are likely due to the modification of catalytic properties by an interaction with the support. While there is a small influence on the rate, the composition of the support, or modification by Cs, has no effect on the HDS/olefin hydrogenation selectivity. The olefin hydrogenation conversion increases linearly with HDS conversion, and at high HDS conversion, few olefins remain in the FCC naphtha. Similar to the effect for Cs promotion of MoS_2 on alumina, the addition of K to sulfided CoMo/alumina had little affect on the activity or selectivity for HDS and olefin hydrogenation. Unlike MoS_2 catalysts, however, with sulfided CoMo at less than about 85% HDS conversion, the rate of olefin hydrogenation is low, but it increases rapidly as the sulfur in the naphtha drops below about 300 ppm. Selective HDS of FCC naphtha appears to correlate primarily to the formation of the CoMoS phase, rather than to the basic nature of the support. It is proposed that the enhanced olefin hydrogenation selectivity of CoMo catalysts is due to the competitive adsorption of sulfur compounds, which inhibit adsorption and saturation of olefins in the naphtha.

Key Words: **hydrodesulfurization; olefin hydrogenation; hydrotreating of FCC naphtha; MoS_2 catalysts; CoMo sulfide catalysts; Mo EXAFS; Co EXAFS.**

INTRODUCTION

Since the 1970s, the U.S. Federal government has enacted regulations aimed to produce cleaner burning fuels with the goal of reducing air pollution. Federal regulations have resulted in the introduction of lead-free gasoline, lower evaporative emissions, addition of oxygenates during winter months, and significantly lower levels of sulfur in diesel fuels. While these changes have improved air quality, the U.S. and E.U. petroleum refining industry face further regulatory pressure to decrease the level of sulfur in transportation fuels (1, 2).

Sulfur in gasoline diminishes the efficiency of an automobile's catalytic converter resulting in increased NO_x and hydrocarbon emissions (3). The U.S. national average gasoline contains about 350 ppm S, while nearly one-fourth of the gasoline contains over 500 ppm S (1, 2). Although the 1990 Clean Air Act Amendments led to significant reductions in auto exhaust emissions, the Environmental Protection Agency (EPA) is now considering whether more stringent emission standards will be required in order to achieve the nation's air quality goals. The EPA is proposing to lower the sulfur level in gasoline in the 22 states with the lowest air quality to 150 ppm. In addition, in states where air pollution is minimal, sulfur in gasoline will be reduced to about 300 ppm. Future regulations could possibly restrict sulfur in gasoline to less than 30 ppm (1).

The Fluid Catalytic Cracking (FCC) unit supplies up to 40% of the gasoline pool in a typical refinery. FCC gasoline generally has high levels of sulfur (1500–2500 ppm) and is the source of nearly all the sulfur in gasoline (3, 4). There are several options for lowering sulfur in FCC gasoline (3). For example, hydrodesulfurization of the gasoil leads to a significant reduction in amount of S in the FCC gasoline (3, 4). However, high-pressure gasoil hydrotreating requires significant capital investment (4) and is generally not economic, especially for small refineries.

FCC gasoline is a complex mixture of over 400 organic compounds broadly classified by boiling range and compound type (aromatics, olefins, naphthenes, and paraffins) with high concentrations of olefins in the lighter boiling fractions and high concentrations of aromatics and sulfur with fewer olefins in the heavier fraction (2, 3). Therefore, fractionation and blending of the heaviest components into diesel fuel could reduce the amount of sulfur in gasoline (3). Endpoint reduction alone, however, will not be sufficient to meet the proposed stricter standards and thus is not a long-term solution.

[1] To whom correspondence should be addressed.

0021-9517/00 $35.00

A third option is to hydrotreat FCC gasoline to remove sulfur (3, 4). Because of the higher reactivity of sulfur compounds in naphtha compared to those in gasoil, lower capital investments are required to achieve the same level of sulfur removal. The principal technical problem with hydrodesulfurization of FCC gasoline is that with conventional catalysts, olefin hydrogenation and, therefore, loss of research octane number (RON) accompanies sulfur removal. Generally, in order to meet the lowest S levels proposed, the economic penalty resulting from the loss in octane is prohibitive.

Several patents have reported that sulfided CoMo on basic supports, like magnesium oxide (5–9) or promotion by alkali (10–13) can catalytically convert sulfur with reduced hydrogenation of olefins. The development of a selective naphtha HDS catalyst and process, which leads to removal of S without significant hydrogenation of olefins, could represent an attractive alternative for complying with the environmental regulations.

In this study, the catalytic activity and selectivity for HDS and olefin hydrogenation of FCC naphtha have been determined for MoS_2 (no Co) catalysts on different supports and for a commercial CoMo/alumina catalyst both with and without addition of alkali. The structure of the catalysts has been characterized by EXAFS and XRD. Selective desulfurization is observed for CoMo/alumina but not MoS_2 catalysts and is suggested to result from formation of the CoMoS phase, rather than the basic properties of the support.

EXPERIMENTAL

Catalyst Preparation

MoS_2 catalysts. The Davison grade 644 silica and Catapal SB alumina supports were commercially available spray-dried microspheres. The supports were calcined at 500°C, and the N_2 BET surface area and pore volumes are reported in Table 1. The alumina support was impregnated with sufficient CsOH to give approximately 1 and 2 wt% Cs and recalcined at 350°C. The catalysts were prepared by pore volume impregnation with ammonium heptamolybdate to give about 5 wt% Mo. The catalysts were dried overnight at 100°C and calcined at 350°C. The catalysts were analyzed for Mo and Cs by ICP. The catalysts were presulfided by heating at 1°C/min from room temperature to 350°C at atmospheric pressure in a high flow of 5% H_2S in H_2. Sulfiding was maintained at 350°C for 1 h. The presulfided catalysts were reduced at 350°C in H_2 prior to catalytic testing, XRD, and EXAFS analysis.

TABLE 1

Elemental Analysis and Physical Properties

Catalyst support	Surface area ($m^2 g^{-1}$)	Pore volume ($c^3 g^{-1}$)	Mo wt%	Co wt%	Alkali wt%
Silica	284	1.12	4.7	—	—
Alumina	203	0.42	4.5	—	—
1% Cs–alumina	194	0.38	4.9	—	0.89 (Cs)
2% Cs–alumina	188	0.37	4.8	—	1.74 (Cs)
CoMo/alumina	218	0.40	11.2	3.1	—
CoMo/alumina +2% K	228	0.39	11.2	3.3	2.1 (K)

TABLE 2

FCC Naphtha Characterization

RON	92.0
Basic N, ppm	12
Total N, ppm	80
Sulfur (XRF), wt%	0.1827
GC PIONA	wt%
Tot SAT-naphthene	12.28
Tot SAT-*i*paraffin	11.64
Tot SAT-*n*paraffin	2.30
Tot UNSAT-naphthene	5.55
Tot UNSAT-*i*paraffin	8.76
Tot UNSAT-*n*paraffin	2.93
Tot aromatic	56.53

CoMo/alumina. The CoMo/alumina catalyst, KF-756 (Akzo Nobel), was commercially available. The CoMo catalyst was modified with alkali by impregnation with KNO_3 to give approximately 2.0 wt% K. After impregnation, the catalyst was dried overnight at 100°C and calcined at 350°C for 3 h. The elemental analysis for Mo, Co, K, and the N_2 BET surface area and pore volume are given in Table 1. The catalysts were presulfided as described above.

Pilot plant testing. Approximately 8 g of MoS_2 catalyst (<100 mesh) was loaded into a small, automated pilot plant and heated to 315°C at 27 atm (2.7 MPa) H_2. The feed was a FCC naphtha, obtained from a commercial unit. The properties are given in Table 2. The HDS conversions between 50 and 95% were obtained by varying the hydrocarbon flow rate between 0.4 and 2.5 weight hourly space velocity (WHSV).

The CoMo/alumina catalysts (14/35 mesh) were evaluated at the same H_2 pressure and H_2/hydrocarbon ratio at a WHSV of 3.3 h^{-1}. However, since the activity was much higher than that of the MoS_2 catalysts, the reaction temperature was lowered between 220 to 260°C, and the conversion was varied by adjusting the temperature. Additionally, samples were collected for K modified CoMo/alumina catalyst at 220°C at WHSV's from 0.83 to 3.3 h^{-1}.

For all tests, the catalysts were operated for approximately 7 days prior to collecting performance data. After a change of conditions, no data was collected for 24 h, and samples were collected during the following 3 days. The weight balances were 99%. At the end of the test, the conditions were returned to the original space velocity to test for deactivation. A typical catalyst evaluation took

approximately 3–4 weeks, during which no deactivation was observed.

Hydrocarbon analysis. N_2 was slowly bubbled through the liquid products at ice temperature to out-gas dissolved H_2S. The samples were analyzed for total sulfur by XRF. A multicolumn GC method was used to determine the paraffin, isoparaffin, olefin, naphthene, and aromatic (PIONA) composition for the C_5–C_{11} hydrocarbons. Research octane numbers (RON) were measured at the BP Amoco auto lab.

Catalyst Characterization

XRD. The XRD diffraction patterns of the presulfided catalysts were measured at ambient conditions on a Scintag PAD V diffractometer equipped with an Ortec intrinsic Ge detector. Unfiltered Cu$K\alpha$ radiation at a tube power of 40 kV and 30 mA was used with monochromation affected in the detector. The data were collected by scanning 2θ between 3 and 90° at step increments of 0.04° and counting for 24 s/step. The strongest MoS_2 peak is at 14.4°, which is also free from interference by alumina peaks. Attempts to perform a Rietveld refinement including this MoS_2 peak was unsuccessful due to the overlap with the support, which could not be fit with an ordered model. As a result, the MoS_2 crystallite sizes were estimated from the Scherrer equation. The peaks were fit with pseudo-Voigt profiles and the instrumental FWHM were subtracted from the fitted half-widths.

EXAFS data collection and analysis. The EXAFS measurements were made at the Materials Research Collaborative Access Team (MRCAT) insertion device beam line at the Advanced Photon Source at Argonne National Laboratory. Measurements were made in transmission mode with ionization chambers optimized for maximum current with linear response ($\sim 10^{10}$ photons detected/s). A double-crystal Si (111) monochromator with resolution of better than 4 eV at 20 keV was used in conjunction with a Pt-coated mirror to minimize the presence of harmonics. The integration time per data point was 1–3 s and 3 scans were obtained for each catalyst.

The sample thickness was chosen to give an absorbance of about 1.0 in the Mo edge region, approximately 0.5 g of presulfided MoS_2 (or 0.2 g of CoMo/alumina). The sample was centered in a 45 × 2 cm, continuous-flow, *in situ* EXAFS cell fitted with Kapton windows. Prior to the EXAFS measurements, the presulfided catalysts were heated to 350°C for 1 h at atmospheric pressure in a flow of 5% H_2 in He (150 cc/min). The EXAFS data were collected at room temperature in 5% H_2/He.

Due to the strong absorption of the Mo and the support in the CoMo/alumina catalyst, great care was taken to provide an extremely uniform sample and eliminate higher order harmonics in the beam. To assure uniformity, the finely ground sample (<100 mesh) was pressed into a wafer between polished steel die. The Co absorption edge step, $\Delta\mu x$, was 0.6 with a total sample absorption coefficient, μx, greater than 3.5 above the edge.

Standard procedures were used to extract the EXAFS data from the absorption spectra using WINXAS97 software (14). Phase shifts and backscattering amplitudes were obtained from the reference compounds, MoS_2 (15) for Mo–S and Mo–Mo, CoS_2 (16) for Co–S. Experimental reference spectra were also compared with theoretically calculated spectra from FEFF 7.0 (17). In particular, the Co–Mo reference file was also generated using FEFF. The amplitude factor was determined by comparing the amplitudes of the experimental Mo–S and Mo–Mo reference spectra with the corresponding FEFF spectra.

RESULTS

HDS and Olefin Hydrogenation of FCC Naphtha

MoS_2 supported on alumina and silica. Figure 1a shows the first-order HDS plot for each of the MoS_2 catalysts.

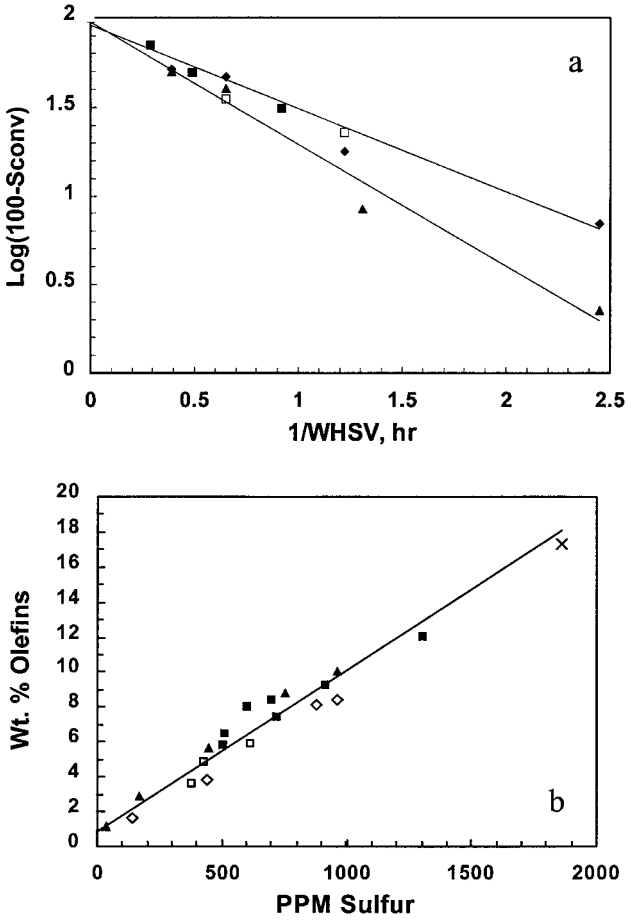

FIG. 1. (a) First-order HDS kinetics, Log(100-S_{conv}) verses 1/WHSV, and (b) olefin hydrogenation versus sulfur conversion. ▲ MoS_2/silica, ■ MoS_2/alumina, □ MoS_2/1% Cs-alumina, ◇ MoS_2/2% Cs-alumina, and ✕ FCC naphtha.

Comparison of the first-order rate constants for HDS indicates that MoS_2 on silica is more active (per g catalyst) than the MoS_2 on alumina(s). Addition of Cs had little effect on the activity of Mo/alumina up to about 2 wt%. Normalization by the amount of Mo gives the relative specific activities, e.g., alumina(s) (1.0) and silica (1.4). The estimated repeatability is ca. 0.1.

The total (linear, branched, and naphthene) olefin hydrogenation conversion as a function of S conversion for all catalysts is shown in Fig. 1b. As S conversion increases, there is a linear increase in olefin saturation. At 100% S removal, there would be nearly complete saturation of the olefins in the naphtha. Within the repeatability of the measurements, Fig. 1b indicates that there is no effect of the support composition, physical properties, or Cs addition on the olefin selectivity.

CoMo/alumina catalysts. Figure 2a shows the first-order HDS kinetics for the K modified CoMo/alumina catalyst at 27 atm and 220°C. At the lowest WHSV of 0.8 h^{-1}, the HDS conversion is 98%, or 40 ppm S in the product. Also shown is the conversion for the CoMo/alumina catalyst at the same temperature and 3.3 h^{-1} WHSV. The HDS conversion is 60% (750 ppm), identical to that of the catalyst with alkali.

At 3.3 h^{-1} WHSV, the HDS conversion was varied by changing the reaction temperature between 220 and 260°C. The results are given in Table 3 along with the RON and the concentration of olefins remaining in the product. At each temperature, the product sulfur, olefins, and RON are very similar, indicating that the addition of K has no effect on the activity of the CoMo/alumina catalyst.

A comparison of the rate of olefin hydrogenation with HDS is given in Fig. 2b for sulfided CoMo with and without K. Up to about 85% S conversion, or 300 ppm S in the product naphtha, the olefin hydrogenation conversion is relatively low. As S conversion increases beyond about 300 ppm, however, the rate of hydrogenation increases rapidly. At complete removal of S, there are few olefins remaining in the product. As observed for the unpromoted MoS_2/alumina catalyst, the addition of alkali has little effect on the olefin hydrogenation/HDS selectivity of sulfided CoMo/alumina. Included in Fig. 2b are the data taken at 220°C and at higher temperatures (at constant WHSV).

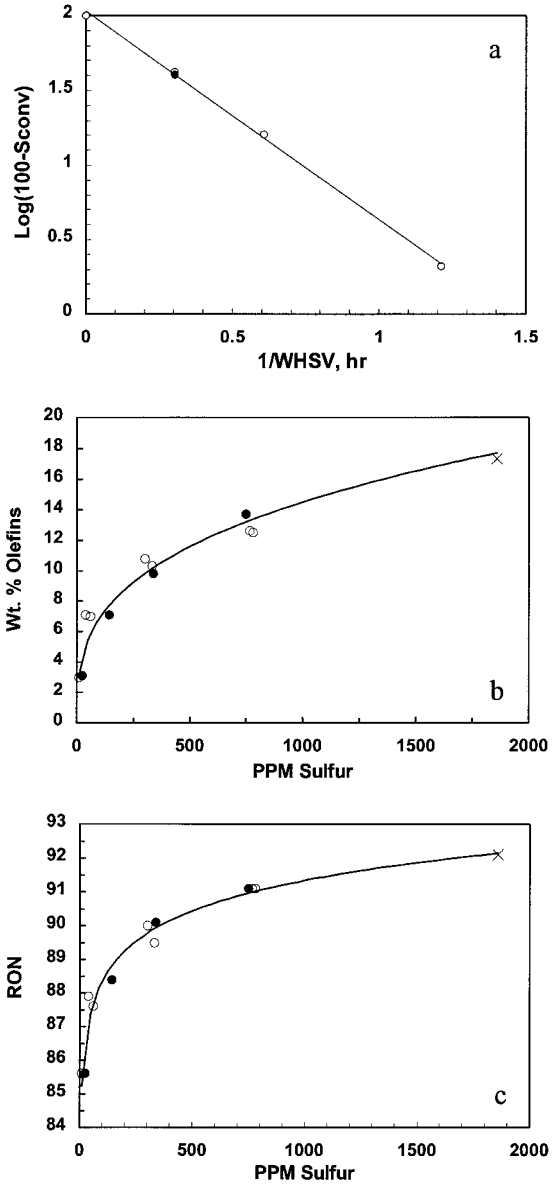

FIG. 2. (a) First-order HDS kinetics, Log(100-S_{conv}) verses 1/WHSV, (b) olefin hydrogenation versus sulfur conversion, and (c) RON verses sulfur conversion. ● CoMo/alumina, O CoMo/2% K-alumina, and ✕ FCC naphtha.

TABLE 3

HDS and Olefin Hydrogenation of FCC Naphtha at 3.3 WHSV and 27 atm

	CoMo/alumina			CoMo/2% K-alumina		
Reaction temperature, °C	S (ppm)	wt% olefins	RON	S (ppm)	wt% olefins	RON
220	750	13.7	91.0	766	12.5	91.1
230	339	9.8	90.1	333	10.3	89.5
245	144	7.1	88.4	93	7.0	87.6
260	24	3.1	85.6	10	3.0	85.6

Figure 2c shows the effect of HDS conversion on RON. Initially, there is a relatively small loss in RON; however, as the sulfur in the product decreases below about 300 ppm, the loss in RON increases. At complete removal of S, there is a loss of about 7 RON in the hydrotreated naphtha. Addition of K did not influence the RON/HDS selectivity.

Catalyst Characterization

Comparison of Figs. 1b and 2b indicate that the olefin hydrogenation/HDS selectivity for supported sulfided CoMo

TABLE 4

EXAFS Fits

Catalyst	Scatter	CN	R, Å	$\Delta\sigma$, Å^2 ($\times 10^{-3}$)	ΔE_o eV
Mo/SiO_2	Mo–S	4.9	2.41	1.74	−0.18
	Mo–Mo	2.6	3.15	1.58	1.00
Mo/Al_2O_3	Mo–S	3.7	2.43	1.74	−0.49
	Mo–Mo	1.7	3.15	1.48	−3.25
$Mo/Cs–Al_2O_3$	Mo–S	4.7	2.42	1.55	1.87
	Mo–Mo	2.7	3.16	2.12	1.50
$CoMo/Al_2O_3$	Mo–S	5.8	2.42	2.02	−0.27
	Mo–Mo	2.6	3.16	1.73	1.78
	Co–S	5.0	2.20	5.91	−5.25
	Co–Mo	1.1	2.80	9.67	−2.78

and MoS_2 are significantly different. In order to determine whether these selectivites are due to differences in structure, the catalyts were analyzed by EXAFS at the Mo and Co edges and XRD.

EXAFS. The Mo K edge EXAFS oscillations were obtained from the X-ray absorption spectra by subtracting a Victoreen curve followed by a cubic spline background removal (18). Energy independent normalization was performed by division by the edge step to give the EXAFS functions. Data analysis of the first Mo–S and Mo–Mo coordination shells for the sulfided Mo and CoMo/alumina catalysts was obtained by an inverse Fourier transform between $r = 1.17$ to 3.23 Å (after Fourier transform: k^2, $\Delta k = 3.01$ to 15.84 Å^{-1}). The reference compounds were analyzed by the same procedure. For each catalyst, 3–4 spectra were obtained and an R-space fit was performed for each data set. The average fit parameters are given in Table 4. The error in the determination of the coordination numbers and distance are less than 5 and 1%, respectively. A typical two-shell fit of the Mo EXAFS for sulfided CoMo/alumina is given in Fig. 3 (solid line: data; dashed line: model fit). Attempts to include a Mo–O contribution resulted in a much poorer fit. There was also no evidence for a Mo–alkali ion contribution to the EXAFS spectra, in agreement with previous studies (19).

Within the experimental error, for all catalysts the Mo–S (2.42 Å) and Mo–Mo (3.16 Å) coordination distances are identical to those in bulk MoS_2 (15), and they agree with previous studies on HDS catalysts (20–24). In the unpromoted MoS_2 catalysts, the Mo–S coordination numbers are slightly lower (between about 4 and 5) than those in sulfided CoMo (5.8). The Mo–Mo coordination numbers between 1.7 and 2.7 agree with previous studies (20–24) and indicate that the MoS_2 domains are small (20–25).

For the CoMo/alumina catalyst, the EXAFS was also obtained at the Co edge. Data analysis of the first shell Co–S was obtained by an inverse Fourier transform between $r = 1.03$ to 2.39 Å (after Fourier transform: k^2, $\Delta k = 2.83$ to 11.74 Å^{-1}). Comparison of the model fit (dashed line) to the experimental data (solid line) for the isolated Co–S coordination is shown in Fig. 4 with the coordination parameters given in Table 4. The bond distance of 2.20 Å is similar to previous EXAFS determinations of the Ni–S and Co–S bond distances in HDS catalysts (21–23, 26). The coordination number of 5.0 is also similar to previous values (23, 26).

The Co–Mo contribution to the EXAFS was evaluated by isolation of the coordination shell from the inverse Fourier transform between $r = 2.39$ to 2.89 Å (FT: k^3, $\Delta k = 2.83$ to 11.74 Å^{-1}). The fit parameters are given in Table 4 and

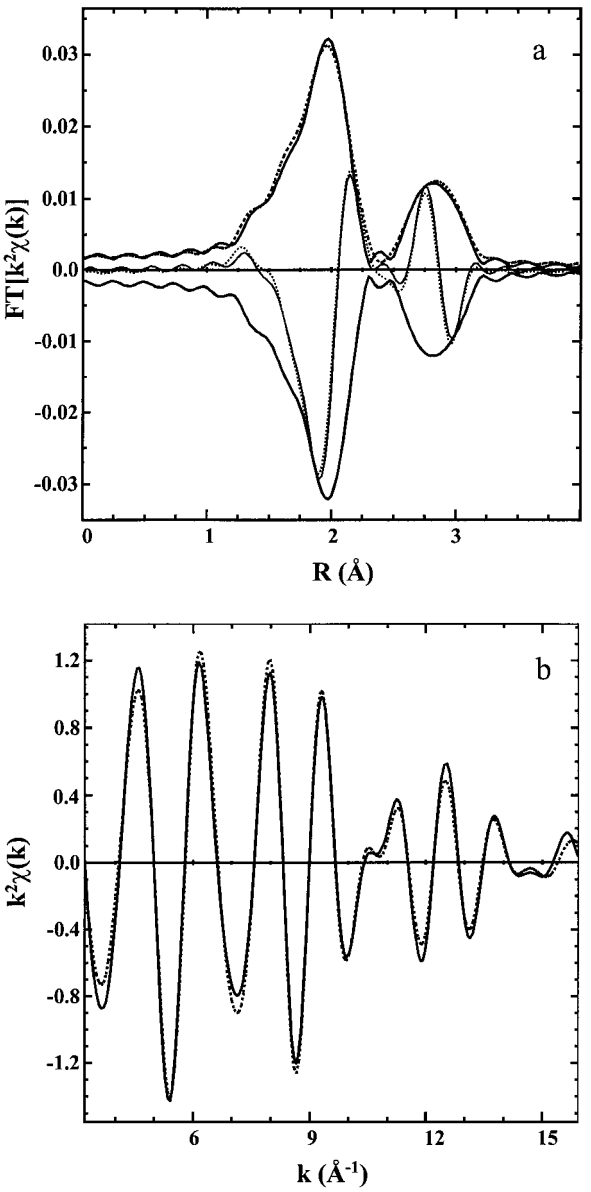

FIG. 3. Mo K edge EXAFS for sulfided CoMo/alumina, k^2, $\Delta k = 3.01$–15.84 Å^{-1}, $\Delta r = 1.17$–3.23 Å: solid line: data; dashed line: model fit. Two-shell fit for Mo–S and Mo–Mo: (a) fit in r space, (b) fit in k space.

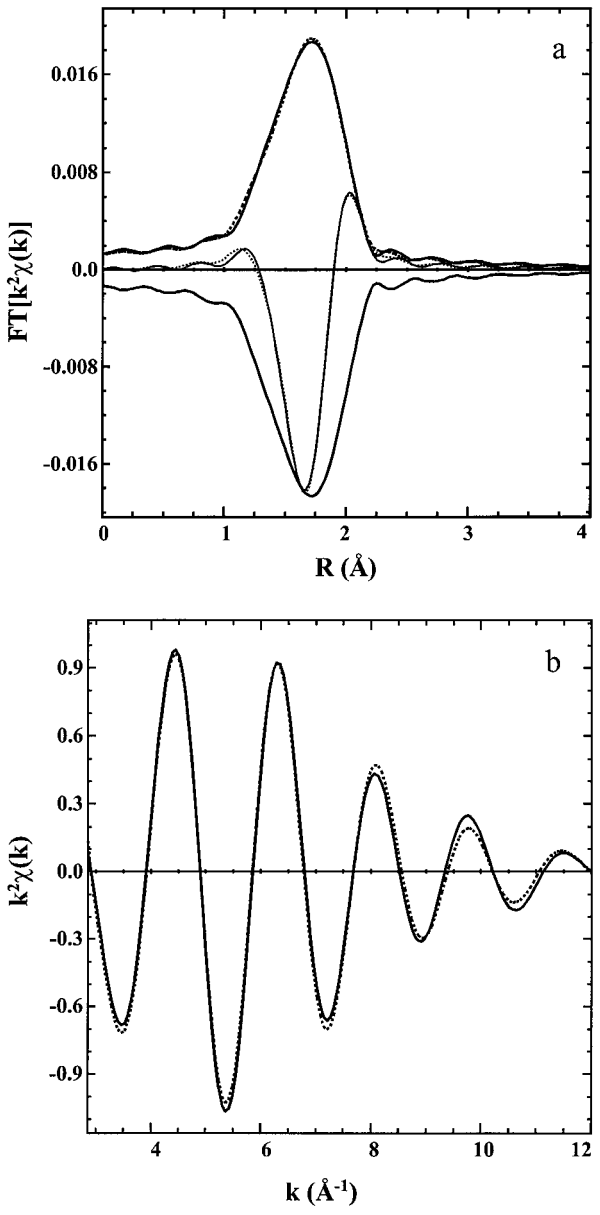

FIG. 4. Co K edge EXAFS for sulfided CoMo/alumina, k^2, $\Delta k = 2.83$–11.74 Å^{-1}, $\Delta r = 1.03$–2.39 Å: solid line: data; dashed line: model fit. Single-shell fit for Co–S: (a) fit in r space, (b) fit in k space.

comparison of the data (solid line) with the model fit (dashed line) is shown in Fig. 5. Since the amplitude of the EXAFS function calculated by FEFF is generally larger than that of experimental references, the amplitude factor, S_o^2, was determined by comparison with experimental references. The Co–Mo coordination distance of 2.80 Å is similar to that in Co(+2) ditetrathiomolybdate (27) and agrees with the Co–Mo and Ni–W coordinations previously reported (21–23, 25, 26). The coordination number of 1.1 is also in good agreement with previous determinations (22, 23, 26).

XRD. The XRD patterns are given in Fig. 6. For MoS_2 on alumina and 2% Cs–alumina, the patterns are identical to that of γ-Al_2O_3. Incorporation of Cs had no discernible effect on the long-range structure of the catalyst. The absence of peaks corresponding to MoS_2 in these two catalysts is consistent with very small particles, i.e., less than about 20 Å. Additional diffraction peaks are observed in the CoMo/alumina at 12.7, 33.4, and 59.3° 2θ. Small peaks at 2θ of 12.7 and 33.4 are shown in expanded scale in Figs. 6a and 6b for MoS_2/silica and CoMo/alumina, respectively, and are consistent with peaks from molybdenite, MoS_2 (28, 29). On CoMo/alumina the peak widths correspond to an

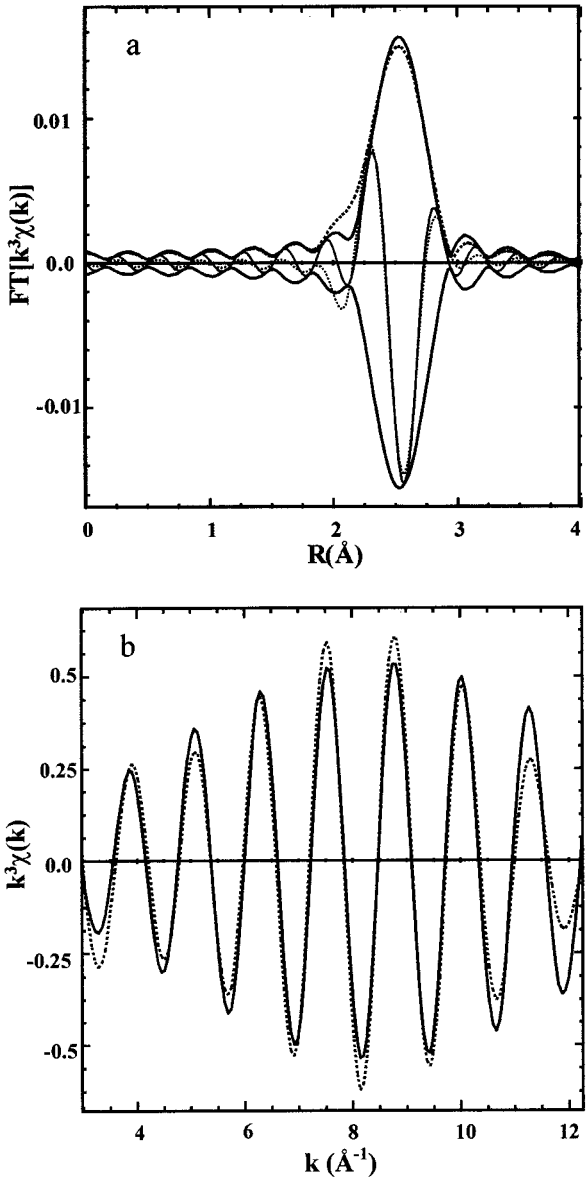

FIG. 5. Co K edge EXAFS for sulfided CoMo/alumina, k^3, $\Delta k = 2.83$–11.74 Å^{-1}, $\Delta r = 2.39$–2.89 Å: solid line: data; dashed line: model fit. Single-shell fit for Co–Mo: (a) fit in r space, (b) fit in k space.

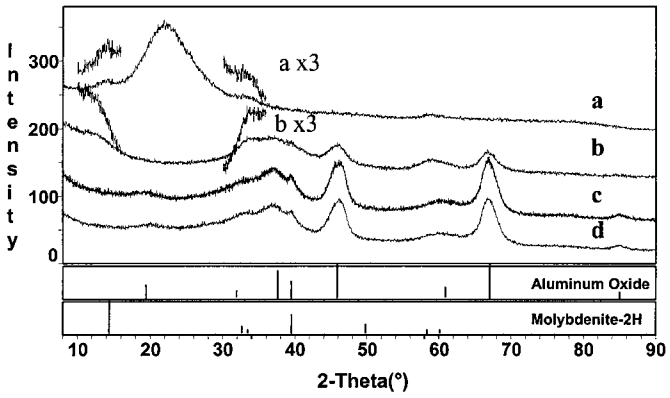

FIG. 6. X-ray diffraction patterns: (a) MoS_2/silica, (b) CoMo/alumina, (c) MoS_2/2% Cs–alumina, and (d) MoS_2/alumina. Reference XRD patterns: Aluminum oxide (10-0425) and Molybdenite-2H (37-1492).

average crystallite domain size of about 20–25 Å. The overlap of the MoS_2 peaks with those of γ-Al_2O_3, make determination of the size anisotropy unreliable. MoS_2 was also detected on the silica-supported catalyst, and the average crystallite size is approximately 35 Å. Again, overlap of the silica pattern precludes reliable determination of the size anisotropy.

DISCUSSION

Gasoline is a mixture of C_5–C_{11} paraffins, olefins, naphthenes, and aromatics. One property, which determines the gasoline value, is its octane number. Generally, octane increases with increasing chain branching, olefin, and aromatic content. Catalytic desulfurization of FCC naphtha results in the loss of octane (RON) with increasing HDS. Figure 7 shows a correlation of the RON with the total (linear, branched, and naphthene) olefin content of the naphtha. The data include all reaction temperatures for both

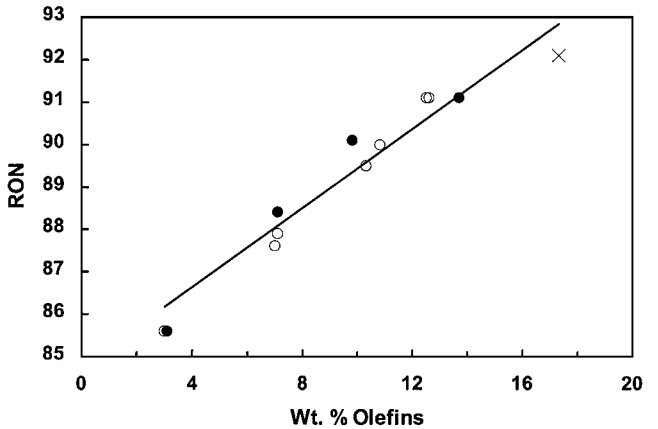

FIG. 7. Correlation of RON with olefin content: ● CoMo/alumina, O CoMo/2% K-alumina, and ✕ FCC naphtha.

CoMo/alumina catalysts. Figure 7 demonstrates that the loss in RON is primarily due to the saturation of olefins. Within experimental error, in the desulfurized gasoline there is no change in the distribution of aromatics indicating little saturation of aromatics. The correlation of RON with the total olefin content suggests there is also little isomerization of paraffins.

The composition of the support has previously been shown to influence the activity of HDS catalysts (30–36). With CoMo catalysts, the activity generally increases in the order alumina > silica (30). For unpromoted MoS_2, the HDS activity on silica is reported to be greater than (32), or slightly lower than (33), that on alumina contrary to results for CoMo. The previous comparisons are complicated by several considerations, however. First, on silica the Mo dispersion decreases with increasing loading (31, 37) and calcination temperature (31). Second, since the activity of MoS_2 is strongly promoted by Co, differences in activity may reflect changes in the degree of Co–Mo interaction, rather than due to an influence by the support. As a result, in order to avoid uncertainties due to the degree of Co promotion, the effect of the support on activity was evaluated for unpromoted MoS_2. In addition, the Mo loading and calcination temperature were kept low in order to maintain high dispersion.

Consistent with previous studies for MoS_2 (32), the specific HDS activity on silica was 1.4 times higher than that on alumina(s). In order to establish that this increased activity is due to an interaction with the support, it also necessary to establish that the composition and structure of the catalytic phase is identical and that the activity is not due to changes in particle size or dispersion. EXAFS and XRD analysis indicates that small MoS_2 particles are present on all catalysts. Thus, the differences in activity are not due to differences in the structure of the catalytic phase.

Previously, the turnover rate (TOR) of HDS catalysts was shown to increase linearly by about a factor of three as the EXAFS Mo–S coordination number increased from about 3 to 5 (38). These data suggest that the TOR is higher for larger MoS_2 particles. Based on this correlation, an increase in the Mo–S coordination number from 3.7 (MoS_2/alumina) to 4.9 (MoS_2/silica) would be expected to increase the TOR by about a factor of 1.5 consistent with the increase in observed activity. However, the Mo–S coordination number of MoS_2/2% Cs-alumina is 4.7, similar to that on silica, but has an HDS activity similar to that on MoS_2/alumina. For these catalysts, therefore, there is no apparent correlation of the EXAFS Mo–S coordination number and specific activity.

Both XRD line broadening and the Mo–Mo EXAFS coordination numbers can be used to estimate the MoS_2 particle size. On MoS_2/alumina and MoS_2/2% Cs–alumina, by XRD the particles are too small to be detected and, therefore, are less than about 20 Å. The particles on

CoMo/alumina are slightly larger, ca. 25 Å, while on MoS_2/silica, the XRD particle size increases to 35 Å. By XRD, only particles larger than about 20 Å are detected. Therefore, since the fraction of large and small particles in MoS_2/silica is unknown, 35 Å represents the largest possible average particle size, although the actual average size could be smaller.

Recent theoretical (39, 40) and experimental (25, 29, 40, 41) studies have shown that determination of the particle size from experimental EXAFS coordination numbers underestimate the actual particle size due to the structural disorder and anharmonic vibration modes of the atoms near the particle surface. As a result, the correlation between the Mo–Mo coordination number and the actual particle size was used to determine the average MoS_2 particle size (40). The particle size of MoS_2 on alumina, silica, CoMo/alumina, and 2% Cs-alumina is estimated to be 15, 20, 20, and 21 Å, respectively. For the alumina-supported catalysts, the EXAFS particle size determinations are generally consistent with the values determined by XRD. In addition, the difference between the average size by XRD and EXAFS for MoS_2/silica suggests that there are only a few larger particles.

The similar particle size determined from EXAFS Mo–Mo coordination numbers for MoS_2/2% Cs-alumina and MoS_2/silica indicate that differences in specific activity are not due to the differences in particle size or dispersion. This conclusion is also supported by comparison of MoS_2/alumina and MoS_2/silica. The specific activity on alumina is lower than that on silica despite the smaller particle size of the former. Since the active phase on each MoS_2 catalyst is identical and the difference in rates is not due to differences in particle size or dispersion, we conclude that the intrinsic MoS_2 activity is affected by the composition of the support. The turnover rate is larger for MoS_2 on silica than alumina by about a factor of 1.4. While silica does enhance the HDS activity slightly, addition of Cs does not have a significant influence on the activity.

There are a number of independent reports, which demonstrate that HDS catalysts on basic supports, for example, those on magnesium oxide or promoted by alkali, display lower olefin hydrogenation selectivity (5–13). Most studies suggest that this enhanced selectivity is due to a significant modification of the catalytic properties by the basic support. In this study, the olefin hydrogenation/HDS selectivity was not influenced by the support composition, nor by incorporation of alkali promoters. This is true for both unpromoted MoS_2 and CoMo catalysts.

While the support composition/alkalinity does not lead to more olefin-selective HDS catalysts, neither does the MoS_2 particle size or the support physical properties. For example, the EXAFS particle size of MoS_2/silica, MoS_2/2% Cs–alumina and CoMo/alumina are similar, but only the CoMo catalysts displays lower olefin saturation selectivity. Likewise, the support surface area and pore volume of the MoS_2 and CoMo on alumina are similar; however, CoMo has a lower olefin saturation selectivity, at least at high feed sulfur levels. The only property which correlates with improved olefin/HDS selectivity is promotion by Co.

While modification by Co is the primary factor leading to selective naphtha HDS catalysts, additional factors must also be important since differently prepared CoMo catalysts display slightly different selectivities (5–13). While these additional factors were not addressed in this study, it is likely that the Co/Mo ratio, degree of Co/Mo interaction, or the presence of additional cobalt sulfide phases alter the selectivity. It is speculated that the optimally selective HDS catalysts have a high fraction of Co coordinated at the edge of the MoS_2 particles, i.e., the CoMoS phase (42–44), leaving little exposed Mo. In this CoMo catalyst, nearly all of the Co is present in the CoMoS structure with no detectable amounts of Co_8S_9. In addition, the Co–Mo coordination numbers are consistent with each Co coordinated to 1–2 Mo (22, 23, 26, 42–44). The fact that the Mo/Co molar ratio (from elemental analysis) is also 2 suggests there is little exposed Mo. More work, however, is required in order to determine which of these factors contribute to the selectivity.

While promotion by Co has a strong influence on the olefin hydrogenation selectivity, so also do the process conditions (45). Although olefin hydrogenation and desulfurization kinetics were not studied in detail, Fig. 2 suggests that selective naphtha desulfurization is observed at sulfur levels above 300 ppm. Figures 2b and 2c are consistent with a Langmuir–Hinschelwood kinetic model, where the rate of olefin hydrogenation is faster than HDS but inhibited by sulfur. Further studies, however, will be required to demonstrate that competitive adsorption of sulfur strongly inhibits the rate of olefin hydrogenation and is the origin of selective hydrodesulfurization.

CONCLUSIONS

The specific HDS activity of MoS_2 is slightly higher on silica than alumina supports. By contrast, the addition of Cs does not affect the HDS activity. While there is a small influence on the rate, the composition of the support has no effect on the olefin hydrogenation/HDS selectivity. On unpromoted MoS_2 catalysts, the olefin hydrogenation conversion increases linearly with the desulfurization conversion. At complete removal of sulfur, few olefins remain in the FCC naphtha resulting in a large loss in RON.

For CoMo/alumina catalysts, the activity and selectivity are also not affected by addition of alkali. For these catalysts, at high levels of sulfur in the FCC naphtha, the olefin saturation conversion is low, but it increases rapidly as sulfur levels decrease to below about 300 ppm. Enhanced olefin/HDS selectivity appears to correlate with the

formation of the CoMoS active phase and is not affected by the support composition, support physical properties, or the MoS_2 particle size. We suggest that selective HDS is due to preferential adsorption of sulfur compounds at the active site, thereby inhibiting adsorption and saturation of olefins.

ACKNOWLEDGMENTS

A portion of this work was performed under the auspices of the U.S. Department of Energy, Basic Energy Sciences, Office of Science (DOE-BES-SC) for the use of the Advanced Photon Source and the Office of Fossil Energy under Contract No. W-31-109-Eng-38. The MRCAT beam lines are supported by the member institutions and the U.S. DOE-BES-SC under Contracts DE-FG02-94ER45525 and DE-FG02-96ER45589. The EXAFS cell was adapted from a design developed by UOP. We especially thank S. R. Bare and F. S. Modica of UOP for their valuable help in the design of this cell.

REFERENCES

1. *Chem. Eng. Prog.,* Aug. 20 (1999).
2. Upson, L. L., and Schnaith, M. W., *Oil Gas J.,* Dec. 8, 47 (1997).
3. Nocca, J.-L., Gialella, R. M., Cosyns, J., and Burzynski, J.-P., NPRA AM-95-50 (1995).
4. Martindale, D. C., Antos, G. J., Baron, K., and Bertram, R. V., NPRA AM-97-25 (1997).
5. Yu, A. P., and Myers, E. C., U.S. Patent 4,132,632 (1979).
6. Bertolacini, R. J., and Trevelyan, A., U.S. Patent 4,140,626 (1979).
7. Dai, E., Sherwood, D. E., Martin, B. R., and Petty, R. H., U.S. Patent 5,441,630 (1995).
8. Dai, E., Sherwood, D. E., and Petty, R. H., U.S. Patent 5,340,466 (1994).
9. Sudhakar, C., Cesar, M. R., and Heinrich, R. A., U.S. Patent 5,525,211 (1996).
10. Dai, E., and Sherwood, D. E., U.S. Patent 5,358,633 (1994).
11. Sudhakar, C., Sandford, G. G., Dahlstrom, P. L., Patel, M. S., and Patmore, E. L., U.S. Patent 5,423,976 (1995).
12. Sudhakar, C., U.S. Patent 5,770,046 (1998).
13. Hatanaka, S., Sadakane, O., Hikita, S., and Miyama, T., U.S. Patent 5,853,570 (1998).
14. Ressler, T. J., *J. Physique IV* **7**, C2 (1997).
15. Dickinson, R. G., and Pauling, L., *J. Am. Chem. Soc.* **45**, 1466 (1923).
16. Elliott, N., *J. Chem. Phys.* **33**, 903 (1960).
17. Zabinsky, S. I., Rehr, J. J., Ankudinov, A., Albers, R. C., and Eller, M. J., *Phys. Rev. B.* **52**, 2995 (1995).
18. Cook, J. W., Jr., and Sayers, D. E., *J. Appl. Phys.* **52**, 5024 (1981).
19. Bian, G.-Z., Fu, Y.-L., and Xie, Y.-N., *Catal. Lett.* **40**, 235 (1996).
20. Clausen, B. S., Topsoe, H., Candia, R., Villadsen, J., Lengeler, B., Als-Neilson, J., and Christensen, F., *J. Phys. Chem.* **85**, 3868 (1981).
21. Bouwens, S. M. A. M., Prins, R., de Beer, V. H. J., and Koningsberger, D. C., *J. Phys. Chem.* **94**, 3711 (1990).
22. Bouwens, S. M. A. M., van Veen, J. A. R., Koningsberger, D. C., de Beer, V. H. J., and Prins, R., *J. Phys. Chem.* **95**, 123 (1991).
23. Louwers, S. P. A., and Prins, R., *J. Catal.* **139**, 525 (1993).
24. Leliveld, R. G., van Dillen, A. J., Geus, J. W., and Koningsberger, D. C., *J. Catal.* **165**, 184 (1997).
25. Shimada, H., Matsubayashi, N., Sato, T., Yoshimura, Y., Imamura, M., Kameoka, T., and Nishijima, A., *Catal. Lett.* **20**, 81 (1993).
26. Louwers, S. P. A., and Prins, R., *J. Catal.* **133**, 94 (1992).
27. Sotofte, I., *Acta Chem. Scand. A* **30**, 57 (1976).
28. Chianelli, R. R., Prestiridge, E. B., Pecoraro, T. A., and DeNuefville, J. P., *Science* **203**, 1105 (1979).
29. Calais, C., Matsubayashi, N., Geantet, C., Yoshimaura, Y., Shimada, H., Kishijima, A., Lacroix, M., and Breysse, J., *J. Catal.* **174**, 130 (1998).
30. Massoth, F. E., Muralidhar, G., and Shabtai, J., *J. Catal.* **85**, 53 (1984).
31. Massoth, F. E., Muralidhar, G., and Shabtai, J., *J. Catal.* **85**, 44 (1984).
32. Shimada, H., Sato, T., Yoshimura, Y., Hiraishi, J., and Nishijima, A., *J. Catal.* **110**, 275 (1998).
33. Pratt, K. C., Sanders, J. V., and Christov, V., *J. Catal.* **124**, 416 (1990).
34. Breysse, M., Portefaix, J. L., and Vrinat, M., *Catal. Today* **10**, 489 (1991).
35. Virnat, M., Hamon, D., Breysse, M., Durand, B., and des Courieres, T., *Catal. Today* **20**, 273 (1994).
36. Afanasiev, P., Geantet, C., and Breysse, M., *J. Catal.* **153**, 17 (1995).
37. Nag, N. K., *J. Phys. Chem.* **91**, 2324 (1987).
38. Boudart, M., Sanchez Arrieta, J., and Dalla Betta, R., *J. Am. Chem. Soc.* **105**, 6501 (1983).
39. Clausen, B. S., Grabek, L., Topsoe, H., Hansen, L. B., Stoltze, P., Norskov, J. K., and Nielsen, O. H., *J. Catal.* **141**, 368 (1993).
40. Shido, T., and Prins, R., *J. Phys. Chem. B* **102**, 8426 (1998).
41. Startsev, A. N., and Kouchubei, D. I., *Kinet. Catal.* **35**, 43 (1994).
42. Topsoe, H., and Clausen, B. S., *Catal. Rev. Sci. Eng.* **26**, 395 (1984).
43. Topsoe, H., Clausen, B. S., Topsoe, N.-Y., and Zeuthen, P., in "Catalysis in Petroleum Refining 1989" (D. L. Trimm, S. Akashah, M. Abshi-Halabi, and A. Brishara, Eds.). Stud. Sur. Sci. Catal., Vol. 53, p. 77. Elsevier, Amsterdam, 1990.
44. Eijsbouts, S., *Appl. Catal. A. Gen.* **158**, 53 (1997).
45. Lapinski, M. P., Riley, K. L., Halbert, T. R., Lasko, W., Kaufman, J. L., Aldridge, C. L., and Touvelle, M. S., WO Patent 97-40120.